Paleomagnetism of the Newcastle Range, northern Queensland: Eastern Gondwana in the Late Paleozoic

Kari L. Anderson[1] and Mark A. Lackie

Department of Earth and Planetary Sciences, Macquarie University, Sydney, New South Wales, Australia

David A. Clark and Phil W. Schmidt

CSIRO Division of Exploration and Mining, North Ryde, New South Wales, Australia

[1]   The Newcastle Range is an extensive (2500 km^2) and well-exposed caldera system erupted on the trailing edge of Eastern Gondwana between 325 and 295 Ma. Paleomagnetic samples were collected from ignimbrites and associated microgranitoid intrusions from the central, northern and southern calderas from which three components of magnetization are recognized. Component 1 is considered to be a viscous magnetization acquired during the Brunhes Chron. A presumed Permian component, C2, is found in seven paleomagnetic sites with a mean pole at 30.9°S, 139.7°E (K = 13.9, A95 = 16.8°, ASD = 21.7°), agreeing with previously reported Permian data from Australia. Carboniferous units have a well-defined characteristic component, C3, distinguished by dual polarity (predominantly reversed) and moderate to steep inclination directions. Paleomagnetic polarities in the Newcastle Range Volcanics are formation dependent and new constraints on the timing of Carboniferous volcanism (~325–317 Ma) are consistent with recent reanalysis of the base of the Permo-Carboniferous Reversed Superchron (PCRS). A mean paleomagnetic pole, calculated from 15 VGPs, lies at 63.4°S, 125°E (K = 26.22, A95 = 7.6°, ASD = 15.8°), suggesting that Australia remained at midlatitudes into the Middle Carboniferous. This paleomagnetic pole is consistent with similarly aged poles from Western Gondwana, the conformity of which indicates contributions from nondipole components of the Earth's paleofield were probably not significant in the time immediately preceding the PCRS.   *INDEX TERMS:* 1525 Geomagnetism and Paleomagnetism: Paleomagnetism applied to tectonics (regional, global); 1540 Geomagnetism and Paleomagnetism: Rock and mineral magnetism; 8157 Tectonophysics: Plate motions—past (3040); 9330 Information Related to Geographic Region: Australia; 9614 Information Related to Geologic Time: Paleozoic; *KEYWORDS:* paleomagnetism, Carboniferous, Australia, APWP, Paleozoic, Gondwana

Citation: Anderson, K. L., M. A. Lackie, D. A. Clark, and P. W. Schmidt, Paleomagnetism of the Newcastle Range, northern Queensland: Eastern Gondwana in the Late Paleozoic, *J. Geophys. Res.*, *108*(B6), 2282, doi:10.1029/2002JB001921, 2003.

1.   Introduction

[2]   Of the Gondwanan continents, Australia is generally regarded as having the best defined apparent polar wander path (APWP) for the Paleozoic [*Van der Voo*, 1993] and serves to define much of Gondwana's movement during this period. Geological evidence supports paleomagnetic data to define an equatorial to subtropical position for Australia during the Late Devonian and into the Early Carboniferous followed by clockwise rotation and a move to high latitudes in the Early Permian [e.g., *Li et al.*, 1991; *Li and Powell*, 2001]. The Middle to Late Carboniferous segment of Australia's APWP, however, suffers from a distinct lack of paleopoles, both with respect to quantity and quality, and this segment of the APWP is largely defined by interpolated and syndeformational poles [e.g., *Chen et al.*, 1994; *Li et al.*, 1989; *Li and Powell*, 2001]. For example, the Mount Eclipse Sandstone syndeformational poles, mes1 and mes2 [*Chen et al.*, 1994; *Li et al.*, 1989], do not agree with contemporaneous paleopoles from cratonic West Gondwana, which plot some 20° south when rotated into Australian coordinates. The present study was undertaken in an effort to provide a Middle Carboniferous paleomagnetic pole from cratonic Australia and to address two areas of uncertainty arising from previously published Australian APWPs: agreement with West Gondwana and primary remanence.

2.   Regional Geology

[3]   The Early Carboniferous to Permian (340–270 Ma) Kennedy Volcanic Province of northeastern Australia cuts across much of northern Queensland (Figure 1, inset) and is considered to mark the trailing margin of Eastern Gondwana in the Late Paleozoic [*Oversby and Mackenzie*, 1995].

———————
[1]Now at Department of Earth and Environmental Sciences, Geophysics Section, Ludwig-Maximilians-Universität, Munich, Germany.
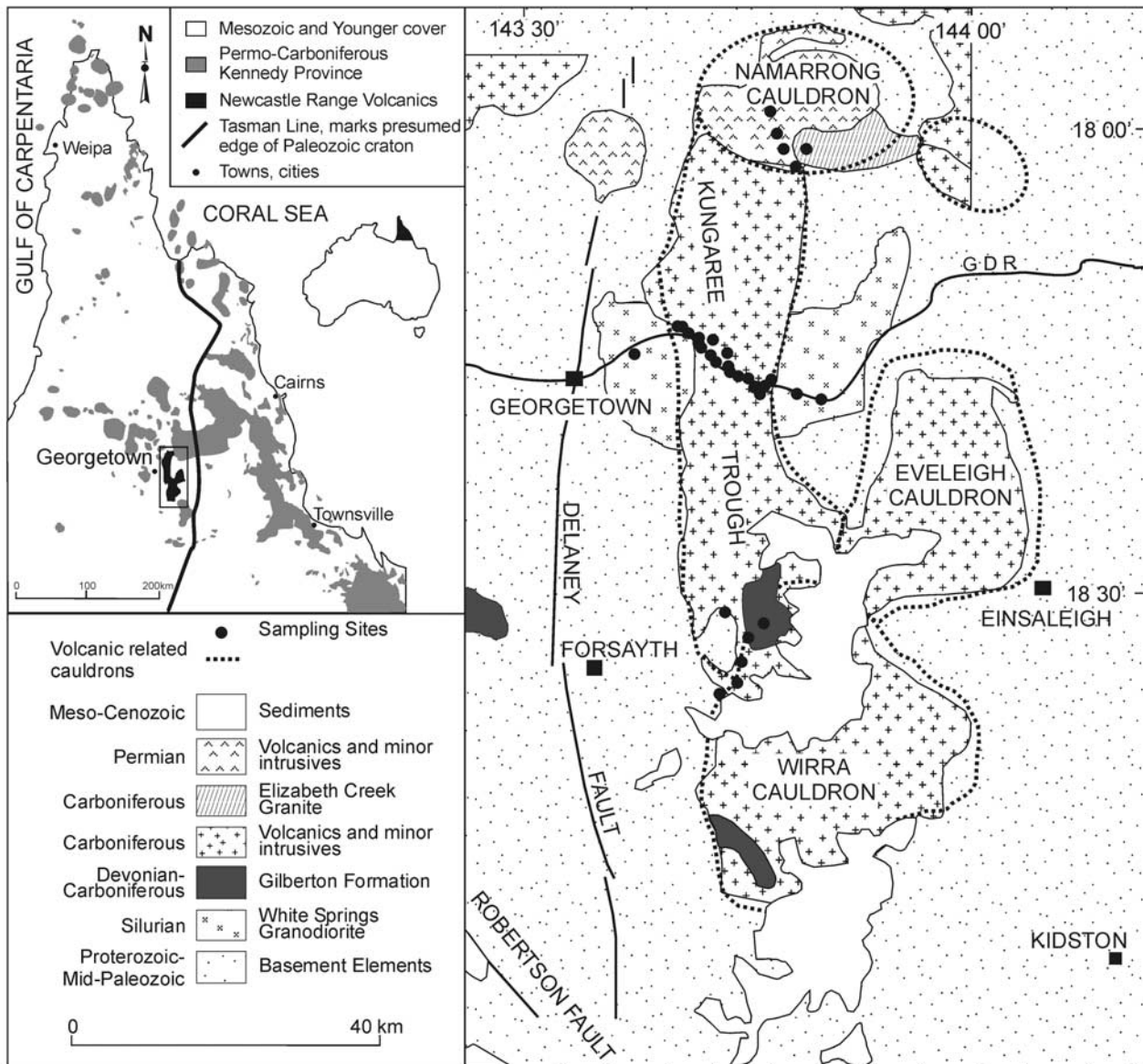
Figure 1. Simplified geological map of the Newcastle Range Volcanics. Map inset in top left corner shows the geographical distribution of Queensland's Carboniferous-Permian Kennedy Volcanic Province and the relation between the NRV and the presumed edge of the Australian (Eastern Gondwanan) craton in the Paleozoic, the Tasman Line. Sampling locations within the Georgetown region (right-hand side of Figure 1) are marked by solid circles. GDR marks the location of the Gulf Development Road in the Georgetown area. Modified from *Oversby and Mackenzie* [1995].

The western margin (present-day coordinates) of the volcanic province is defined by a diffuse distribution of Carboniferous I-type volcanic rocks derived from older, evolved crust, of which the Newcastle Range is a well-preserved remnant located west of the presumed eastern edge of the Paleozoic Australian craton, marked by the Tasman Line.

[4]   The Newcastle Range is an extensive (2500 km²) and well-exposed complex of calderas, running roughly north-northeast for 150 km (Figure 1). Overlap and interfingering relationships between volcanic units afford moderate to good stratigraphic correlation between the central, southern and northern lobes within the caldera complex [*Oversby and Mackenzie*, 1995]. Contacts between the Newcastle Range Volcanics (NRV) and the underlying Devonian – Carboniferous lacustrine sediments of the Gilberton Formation grade from conformable to disconformable whereas angular unconformities occur between the NRV and Silurian White Springs Granodiorite and Proterozoic basement [*Oversby and Mackenzie*, 1995].

[5]   Where observed, bedding of the ignimbrites was generally subhorizontal, dips <5°, indicative of the region having experienced very little, if any, deformation since the Middle Carboniferous and current horizontal, therefore, is

assumed to reflect paleohorizontal across all formations. The only significant dips (>10°) observed in the field were associated with a near-vertical ring dike sampled at the eastern margin of the Kungaree Trough. Lithologically, the area is dominated by subaerially deposited A- and I-type welded rhyolitic ignimbrites, purple to gray in color. Contemporaneous lava flows and microgranitoid intrusions are common. Variably developed ring dikes divide the preserved basinal structures of the volcanic complex into eastern, northern, and southern lobes linked by a central trough-like structure (the Eveleigh, Namarrong, and Wirra Cauldrons and the Kungaree Trough, respectively) [*Oversby and Mackenzie*, 1995].

3. Sampling Details and Laboratory Methods

[6] Thirty-two sites near Georgetown in far north Queensland (Figure 1) were sampled for paleomagnetic investigation. Block samples (three to seven per site) were collected at all sites and generally oriented using both magnetic and sun compasses. Exposure ranges from fair to excellent in this region, particularly along the Gulf Development Road where 18 of the 22 Carboniferous sites were collected. Sampling was also conducted at four sites in the Early Permian Brodies Gap Rhyolite for comparison with the well-defined Mount Leyshon Igneous Complex/ Tuckers Range Volcanics paleopole [*Clark and Lackie*, 2003]. A site from the 308 Ma Elizabeth Creek Granite, two sites in the Devonian–Carboniferous Gilberton Formation and three sites from the Silurian White Springs Granodiorite were sampled to evaluate the thermochemical effects of the emplacement of the NRV in the region. Approximate stratigraphic relations between Permian and Carboniferous volcanic formations with the underlying Gilberton Formation are shown in Figure 2. Sites within the White Springs Granodiorite, Elizabeth Creek Granite,

and Corkscrew Rhyolite did not yield consistent paleomagnetic results and are not considered further.

[7] In the laboratory, two to four 2.5 cm diameter cores were taken from each block with one to four specimens (2.2 cm in height) cut from each core. Prior to demagnetization procedures, bulk rock susceptibility and anisotropy of magnetic susceptibility (AMS) were measured for all specimens. Intensities and directions of the natural remanent magnetization (NRM) were determined using a horizontally
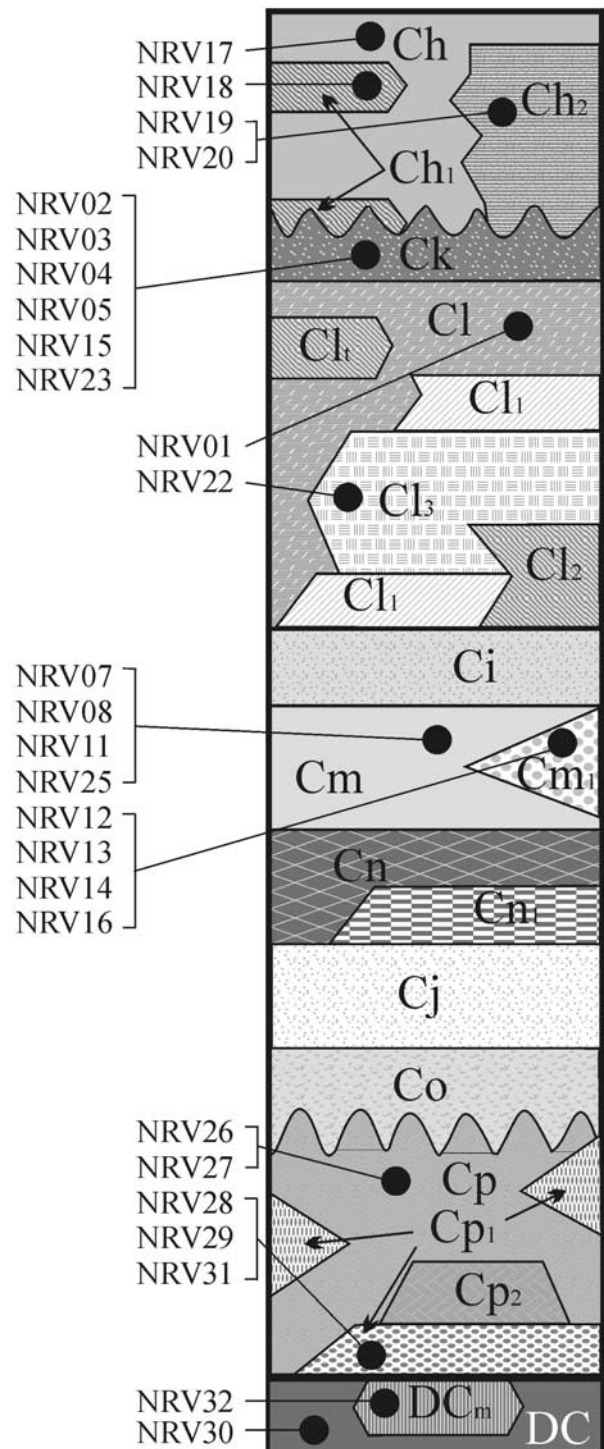

Figure 2. (opposite) Simplified volcanostratigraphy of the Newcastle Range Volcanics. Solid circles represent relative stratigraphic levels of paleomagnetic sites. For purposes of clarity, only one solid circle is shown for each stratigraphic level and may represent more than one paleomagnetic site. Volcanic formation names are as follows (subscript numerals in stratigraphic column represent members of the named formations): Ch, Brodies Gap Rhyolite (293 ± 3 Ma); Ck, Kitchen Creek Rhyolite (317 ± 6.3 Ma); Cl, Corkscrew Rhyolite; Cm, Routh Creek Dacite (322 ± 6.3 Ma); Ci, Dagworth Andesite; Cn, Shamrock Rhyolite; Cj, Twin Dams Andesite; Co, Jinker Creek Rhyolite; Cp, Bousey Rhyolite (325 ± 3 Ma); DC, Gilberton Formation; DCm, Mambera Andesite Member of DC. Ci, Cn, and Cj were not sampled during this investigation. Also, although sampling location within Cl is shown, samples from this rhyolite did not yield consistent paleomagnetic results and were not included in any analyses. Maximum cumulative stratigraphic thickness of the NRV is 8000–10,000 m. (Dates of volcanic sequences were obtained from L. P. Black, as cited by *Oversby and Mackenzie* [1995] (Bousey Rhyolite), and as a part of this study (Kitchen Creek Rhyolite and Routh Creek Dacite).)

mounted 2G755R DC SQUID magnetometer in the Rock Magnetism laboratory at Commonwealth Scientific and Industrial Research Organisation (CSIRO) in Sydney. At least two specimens per block sample were subjected to stepwise thermal and/or alternating field (AF) demagnetization reaching maximum temperatures and fields of 700°C and 160 mT, respectively. Analysis of pilot runs indicated that thermal demagnetization was more effective than AF for the separation of distinct paleomagnetic components of the NRV and so was used as the primary demagnetization method. In addition, following the preliminary measurements, all specimens were subjected to low-temperature demagnetization (cooling in a liquid nitrogen bath and rewarming to room temperature in zero field (LN_2 step)) prior to thermal demagnetization in an effort to reduce magnetizations carried by multidomain magnetite or lightning induced remanence [*Schmidt*, 1993].

[8] Demagnetization behavior was monitored throughout the experiments via visual inspection of orthogonal vector diagrams [*Zijderveld*, 1967] and equal-area stereographic projections. Principal component analysis [*Kirschvink*, 1980] was used to determine characteristic and secondary magnetization components. Specimens for which components had maximum angular deviation (MAD) >10° or those displaying chaotic behavior were not included in later analyses. Site-mean directions of the remaining well-defined magnetizations were calculated according to standard methods [*Fisher*, 1953] as a quantile-quantile analysis of calculated VGPs showed that a Fisher distribution for this data set is valid at the 95% confidence interval [*Tauxe*, 1998]. Filtering of the resultant paleomagnetic data consisted of a two-step process, wherein samples lacking between-specimen consistency were rejected from further analysis. At the site level, samples not displaying within-site consistency were discarded, as were sites with fewer than three remaining samples. Site level virtual geomagnetic poles (VGPs) were calculated when minimum-filtering criteria had been met.

[9] Remanence carriers were identified by thermal and AF demagnetization behavior, hysteresis curves, coercivity spectra, isothermal remanent magnetization (IRM), saturating field thermal magnetization (Js-T) and thermal demagnetization of three component isothermal remanent magnetization (3D-IRM). Js-T, IRM, coercivity spectra and hysteresis curve experiments were performed using a Magnetic Measurements variable field translation balance (VFTB), manufactured by the University of Munich. For the stepwise thermal demagnetization of 3D-IRM [*Lowrie*, 1990], the following fields were applied to each specimen: 1 T along the *z* axis, 0.1 T along the *y* axis, and 0.01 T along the *x* axis.

4. U-Pb Dating

[10] Laser ablation microprobe inductively coupled plasma mass spectrometry (LAM-ICPMS) analyses of U-Pb ratios in zircons from the Routh Creek Dacite (RCD) and Kitchen Creek Rhyolite (KCR) were performed as a part of this study to better constrain the timing of Carboniferous volcanism within the Newcastle Range caldera complex. LAM-ICPMS facilities are housed within the Australian National Key Centre for the Geochemical Evo-lution and Metallogeny of Continents (GEMOC), Macquarie University. Details of the analytical techniques for this dating method are given by *Belousova et al.* [2001]. Results from eleven zircons from the RCD and six from the KCR provided data suitable for age analysis (K. L. Anderson, manuscript in preparation, 2003). LAM-ICPMS U-Pb dating of the RCD yielded an age of 321.9 ± 6.6 Ma (2σ) and that of the KCR of 316.9 ± 6.3 Ma (2σ). Although relatively poorly constrained, these ages are consistent with the U-Pb (sensitive high-resolution ion microprobe, SHRIMP) date obtained for the Bousey Creek Rhyolite of 323 ± 3 Ma (L. P. Black, as cited by *Oversby and Mackenzie* [1995]). These dates also corroborate the emplacement of these formations prior to and during the initial stages of the PCRS as recently redefined by *Opdyke et al.* [2000].

5. Results
5.1. Rock Magnetic Results

[11] An AMS investigation of the NRV was carried out using a low-field Digico Anisotropy Delineator, interfaced to a PC. Figure 3 shows a lower hemisphere projection of principal directions of the AMS ellipsoid for representative sites within the NRV, bootstrapped confidence ellipses with means for respective data sets and also histograms of the relative magnitudes of eigenvalues determined by performing site parametric bootstrap analyses [*Constable and Tauxe*, 1990; *Tauxe*, 1998]. Figures 3a and 3b reveal oblate fabrics, evidenced by the grouping of the minimum susceptibility axes and a girdling of the intermediate and minimum axes. This fabric can be seen statistically on associated histograms, where τ3, bootstrapped eigenvalues associated with the minimum axes, dominates while τ2 and τ1 are statistically indistinguishable, demonstrated by the overlapping of the associated confidence bounds (τ1 ≈ τ2 > τ3) [*Tauxe*, 1998]. Prolate fabrics (τ1 > τ2 ≈ τ3) are shown in Figures 3c and 3d for the ignimbrites associated with the NRV, while Figures 3e and 3f illustrate triaxial fabrics (τ1 > τ2 > τ3) by tight grouping of the three principal susceptibility axes. Table 1 lists the directions of the three principal susceptibility axes, determined via bootstrap analysis, the relative magnitudes of the eigenvalues determined from each site parametric bootstrap analysis, and the shape of the susceptibility ellipsoid determined at each site [*Constable and Tauxe*, 1990; *Tauxe*, 1998].

[12] While within-site AMS results were consistent and well defined, directions across the caldera system were complex and difficult to interpret with regards to local structure or possible volcanic source locations. Analysis of the AMS data from the transect across the center of the Kungaree Trough (Figure 1), for example, failed to detect any possible "settling-in" structures related to caldera collapse, nor were potential source locations identified. As neither structure nor flow directions were discerned by the AMS investigation, and indeed magnetic fabrics are classified as oblate, prolate, or triaxial on a site-by-site basis, it is thought that the inability to reconcile magnetic fabrics across the complex is perhaps indicative of turbulent flow and/or significant paleotopography during eruption. It is possible that a more detailed AMS investigation would more fully reveal structure recorded by magnetic mineralogy and/or source vent locations.
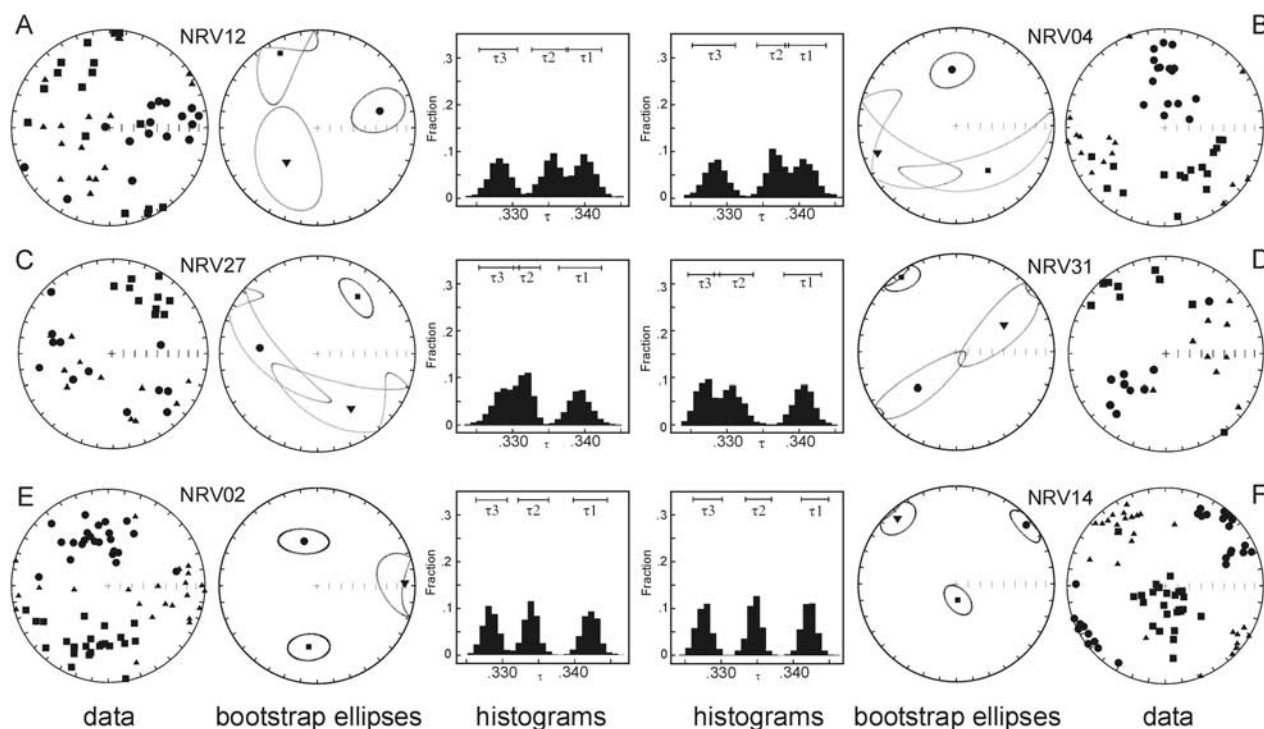
Figure 3. Representative AMS data for the NRV. Stereoplots are lower hemisphere equal-area projections of the K_{max}, K_{int}, and K_{min} axes of the susceptibility ellipsoid, squares, triangles, and circles, respectively. Center stereonets for each subset (a–f) show bootstrapped eigenvectors and associated 95% confidence ellipses generated by the site parametric bootstrap. Histograms illustrate the corresponding bootstrapped eigenvalues, where $\tau 1$, $\tau 2$, and $\tau 3$ refer to maximum, intermediate and minimum susceptibilities along the K_{max}, K_{int}, and K_{min} axes. Histograms and stereonets are modified from s_hist.exe and plotams.exe [*Tauxe*, 1998]. AMS data for all analyzed Permian and Carboniferous formations are listed in Table 1. The three Carboniferous volcanic formations are represented by NRV04(B) and NRV02(E), Kitchen Creek Rhyolite; NRV12(A) and NRV14(F), Routh Creek Dacite; and NRV31(C) and NRV27(D), Bousey Rhyolite.

[13] Identification of remanence carrier mineralogy and structure was accomplished via a series of rock magnetic tests performed on at least one specimen per site using the VFTB. Investigation techniques included bulk rock hysteresis curves, isothermal remanent magnetization (IRM), coercivity spectra and saturating field ($\sim$0.78 T) thermal magnetization (Js-T), in air up to 700°C. Typical results for the NRV include IRM curves fully saturated by the maximum field ($\sim$0.78 T) and moderate backfield coercivity values, $\sim$45 mT (Figure 4). Curie temperatures determined from Js-T investigations, range between 550°C and 600°C across all formations with suggestions of an additional Curie point between 625°C and 655°C for some samples (Figures 5a–5c).

[14] Demagnetization spectra of the 3D-IRM were used to determine the relative contribution from magnetic carriers of varying coercivities, i.e., hard ($>$0.1 T), medium (0.01–0.1 T), and soft ($<$0.01 T). The 3D-IRM demagnetization indicates that remanence carriers for the NRV are mixed. The intermediate coercivity component is the dominant remanence carrier for the NRV, supporting coercivity results gained from the VFTB, but the high-coercivity component also carries a comparatively high proportion of the remanence. Differences in unblocking temperatures (T_{ub}) determined from the 3D-IRM and Js-T analyses are highlighted by comparison of Figures 5a–5c and Figures 5d–5f. There is evidence for two discrete unblocking temperatures in the Routh Dacite; one between 560°C and 600°C with another at around 680°C to 700°C, suggesting magnetite and hematite are present in this formation (Figure 5e). However, as the hematite component is not found in all Routh Dacite samples, pseudo single domain magnetite, as detected by hysteresis properties, is thought to be the dominant carrier of primary remanence in this formation.

[15] Samples from the Bousey Rhyolite have 3D-IRM T_{ub}s falling near 650°C (Figure 5f) and Kitchen Creek Rhyolite (Figure 5d) has two 3D-IRM T_{ub}s, 640°C and 680°C. While dominance of medium coercivity minerals (H_{cr} = 100 mT, mean $H_{cr} \sim$ 45 mT) and saturation IRM curves from the VFTB may suggest cation deficient magnetite (CDM) or maghemite as the $\sim$650°C remanence carrier in these formations, this unblocking temperature is slightly higher than the range generally attributed to CDM [*Clark*, 1997] and the lack of inflection on Js-T curves around 350°C precludes maghemite [*Kletetschka et al.*, 2000]. As coercivities for hematite tend to be suppressed

Table 1. Site-Level AMS Results From the NRV[a]

Site	Formation	$\langle\chi\rangle$	K_{max}		K_{int}		K_{int}		$\tau1$	$\tau2$	$\tau3$	Shape of Ellipsoid
			Dec, deg	Inc, deg	Dec deg	Inc deg,	Dec, deg	Inc, deg				
NRV17	BGR	10.1	335.7	47.7	126.3	13.4	218.0	7.3	0.33726	0.33303	0.32972	spherical
NRV18	BGR	11.5	256.7	38.9	4.7	20.8	116.0	43.8	0.33759	0.33355	0.32885	spherical
NRV19	BGR	13.2	260.8	58.7	110.4	27.9	13.3	13.1	0.33895	0.33141	0.32965	spherical
NRV20	BGR	6.8	25.1	47.4	270.1	21.3	164.3	34.9	0.33738	0.33130	0.32949	spherical
NRV10	CPr sill	47.5	275.1	81.0	98.9	9.0	8.8	0.6	0.34303	0.33722	0.31975	oblate
NRV01	CR	2.1	115.0	41.2	262.5	43.9	9.5	16.9	0.33758	0.33538	0.32704	oblate
NRV22	CR	40.1	226.6	16.4	131.3	17.4	357.3	65.7	0.34609	0.34307	0.31084	oblate
NRV02	KCR	44.4	187.6	37.0	88.4	12.0	343.4	50.4	0.34092	0.33253	0.32655	triaxial
NRV03	KCR	37.6	177.4	39.2	62.6	27.2	308.3	38.1	0.33722	0.33193	0.33085	prolate
NRV04	KCR	56.6	145.0	43.6	250.8	16.0	355.8	42.1	0.33894	0.33510	0.32596	oblate
NRV05	KCR	25.1	228.0	40.7	73.2	46.5	329.3	12.9	0.33712	0.33438	0.32850	oblate
NRV15	KCR	101.0	318.5	21.0	57.3	22.2	189.2	58.6	0.33608	0.33528	0.32864	oblate
NRV16	KCR	27.0	237.4	9.7	114.7	72.4	329.9	14.5	0.33821	0.33402	0.32777	oblate
NRV23	KCR	40.3	223.4	7.1	319.2	39.1	124.9	50.0	0.33729	0.33324	0.32947	spherical
NRV26	BR	39.0	0.4	0.1	90.5	29.2	270.2	60.8	0.33577	0.33790	0.33043	spherical
NRV27	BR	26.2	35.0	29.7	148.4	34.9	275.5	40.8	0.33907	0.33157	0.32936	prolate
NRV28	BR	28.0	207.9	22.1	300.8	7.1	47.7	66.7	0.33864	0.33234	0.32902	prolate
NRV29	BR	27.7	104.5	57.1	10.9	2.3	279.4	32.8	0.34110	0.33149	0.32740	prolate
NRV31	BR	0.9	323.7	7.0	60.4	43.8	226.5	45.4	0.34516	0.33132	0.32352	prolate
NRV07	RCD	3.0	17.0	1.2	122.5	85.7	287.0	4.2	0.34474	0.33331	0.32190	triaxial
NRV08	RCD	23.6	228.6	17.8	126.3	33.6	341.7	50.8	0.33949	0.33286	0.32765	spherical
NRV11	RCD	3.0	69.1	31.1	321.4	26.8	198.9	46.8	0.34093	0.33097	0.32810	prolate
NRV12	RCD	102.1	333.5	15.5	222.6	51.4	74.6	34.1	0.33874	0.33424	0.32702	oblate
NRV13	RCD	70.7	42.5	63.3	308.8	1.8	217.9	26.7	0.34190	0.33187	0.32622	prolate
NRV14	RCD	79.6	173.7	76.5	318.5	11.1	50.0	7.6	0.34188	0.33316	0.32497	triaxial
NRV25	RCD	15.4	73.9	31.8	196.2	40.7	320.2	32.9	0.33895	0.33450	0.32655	oblate

[a]Results from AMS analyses for the NRV. Site, sampling site. Formation: BGR, Brodies Gap Rhyolite (293 ± 3 Ma); CR, Corkscrew Rhyolite; KCR, Kitchen Creek Rhyolite (317 ± 6.6 Ma); RCD, Routh Creek Dacite (322 ± 6.3 Ma); CPr is a Carboniferous-Permian sill associated with RCD; BR, Bousey Rhyolite (323 ± 3 Ma). $\langle\chi\rangle$ is site mean bulk susceptibility in SI units (SI × 10^{-6}); K_{max}, K_{int}, and K_{min}, Dec, and Inc columns list the mean declination and inclination of the maximum, intermediate, and minimum principal susceptibility axes, respectively, and were determined by site parametric bootstrap analysis; $\tau1$, $\tau2$, and $\tau3$ are the relative magnitudes of the eigenvalues from the site parametric bootstrap tests; shape of the ellipsoid refers the overall shape of the susceptibility ellipsoid for each site. All applications of bootstrap methods to susceptibility data were carried out via methods described by *Constable and Tauxe* [1990] and *Tauxe* [1998] and available from *Tauxe* [1998].
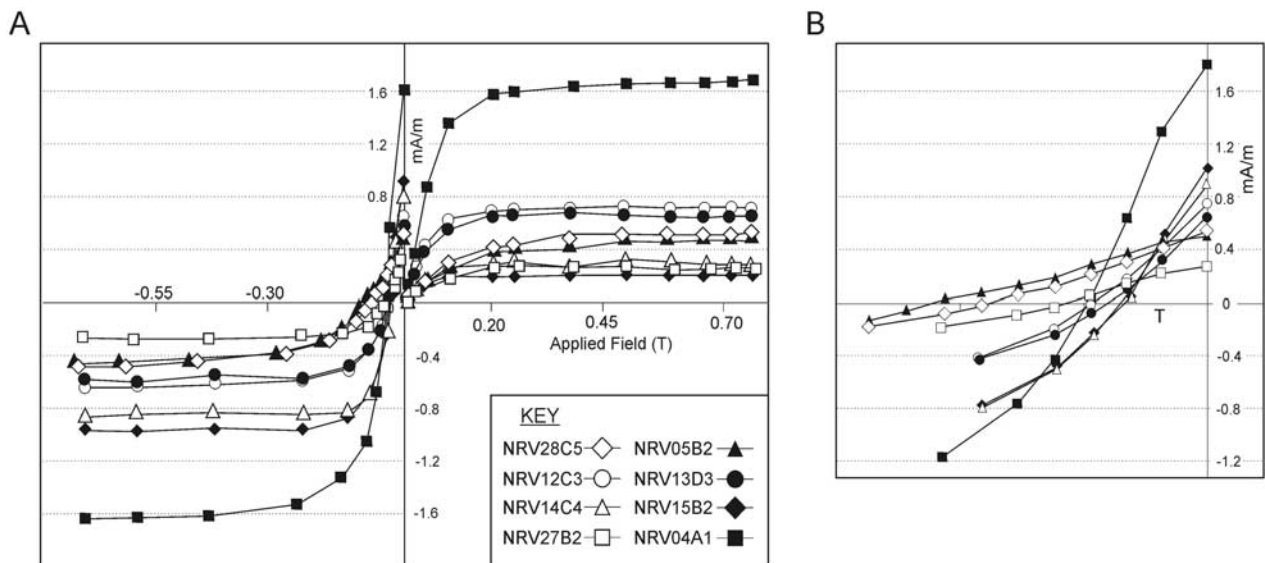

Figure 4. (a) Representative isothermal remanent magnetization (IRM) and coercivity data for the NRV. The IRM and backfield magnetization were imparted to specimens by continuously increasing magnetic fields in the VFTB. Rock magnetic investigations of the NRV indicate that the volcanics have only moderate backfield coercivity values, ~45 mT and, with the exception of NRV04 (a Kitchen Creek Rhyolite example), are fully saturated in laboratory fields (~0.78 T). (b) Details of backfield coercivity values from Figure 5a. Key and vertical axis are as in Figure 4a, but the horizontal axis runs from zero to an applied backfield of −0.12 T. Small ticks on horizontal axis mark 0.04 T increments. The maximum backfield coercivity value is around 90 mT with most samples having values closer to 40 mT. NRV04, NRV05, and NRV15 are Kitchen Creek Rhyolite; NRV12, NRV14, and NRV13 are Routh Creek Dacite; and NRV27 and NRV28 are Bousey Rhyolite.
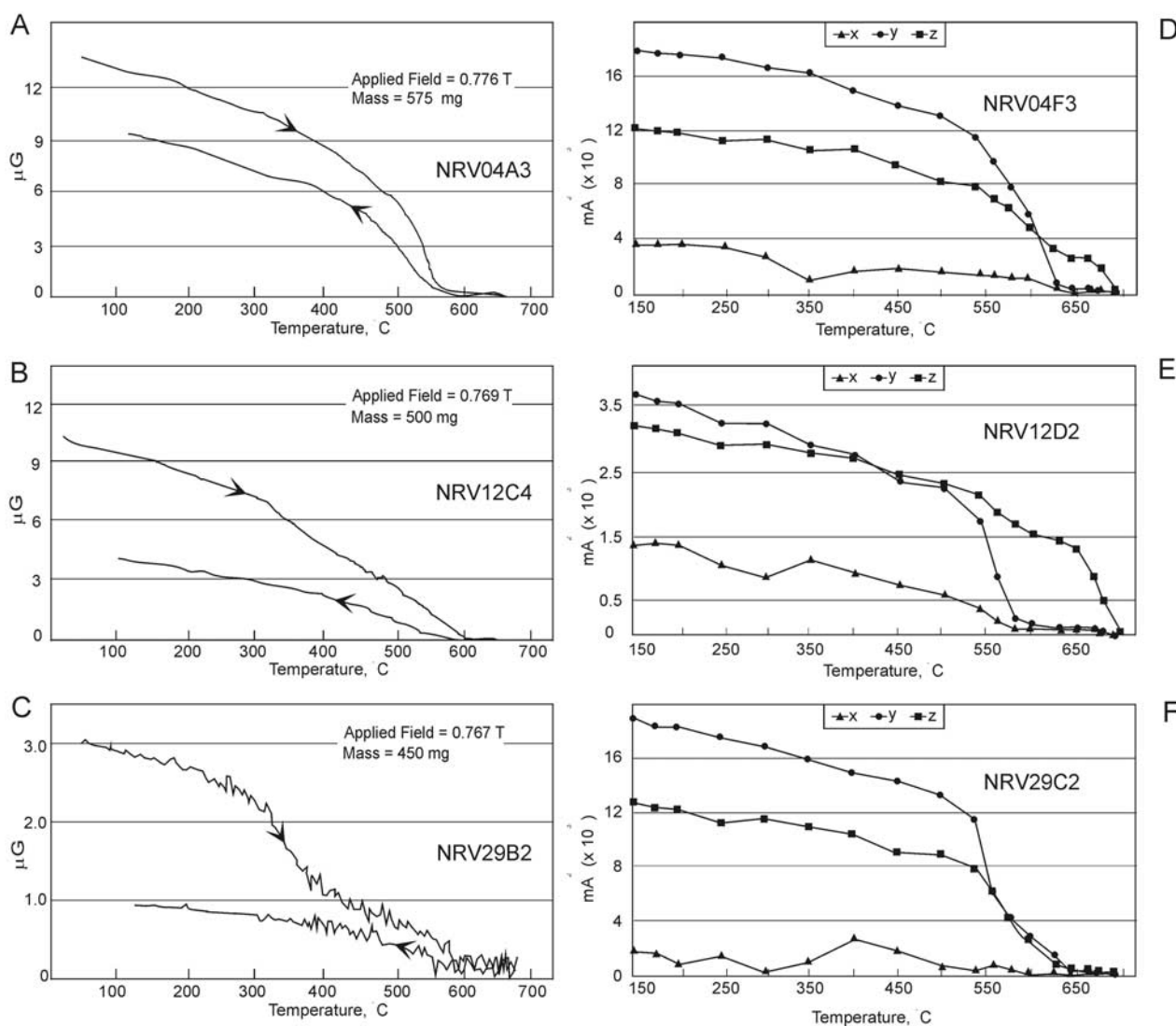
Figure 5. (a–c) Js-T (saturating field demagnetization) and (d–f) 3D-IRM (thermal demagnetization of three-axis IRM [*Lowrie*, 1990]) of representative NRV data. Heating and cooling curves for the Js-T are indicated by directional arrows. Saturating field for all specimens ranged between 0.75 and 0.77 T. Curie temperatures based upon Js-T data fall between 550°C and 600°C across all formations with indications of secondary Curie temperatures between 625°C and 655°C for ignimbrites associated with the Kitchen Creek Rhyolite (Figure 5a) and Routh Creek Dacite (Figure 5b). The 3D-IRM data show that the intermediate coercivity component is dominant in sampled ignimbrites (*y* axis demagnetization curve). The Kitchen Creek Rhyolite, represented by NRV04 (Figure 5d), has two discreet unblocking temperatures 630°C for the low and intermediate coercivity components and 680°C for the high coercivity component. The 3D-IRM tests also revealed two unblocking temperatures for the Routh Creek Dacite (NRV12, Figure 5e), 580°C and 680°C, while all components associated with the Bousey Rhyolite (Figure 5f) unblock simultaneously at ~630°C.

when moving from the single-domain (SD) to the multi-domain (MD) state [*Kletetschka et al.*, 2000], it is suggested that transitional structure hematite is the dominant carrier of magnetization for these two formations. This claim is supported by the presence of hematite grains in the volcanic matrix in the size range of 20–60 μm (Figure 6). The maximum unblocking temperatures, which should correspond closely to Curie temperatures for grains in this size range, suggest that the hematite contains small amounts of titanium, lowering the Curie temperature for

these remanence carriers from that of pure hematite (675°C). This is consistent with the observation that NRM intensities and directions did not change appreciably after cooling in LN$_2$, as small amounts of titanium suppress the Morin transition in hematite [*Dunlop and Özdemir*, 1997].

5.2. Paleomagnetic Results and Interpretations

[16] Three directions of magnetization are present in Carboniferous–Permian units from the NRV (Table 2).
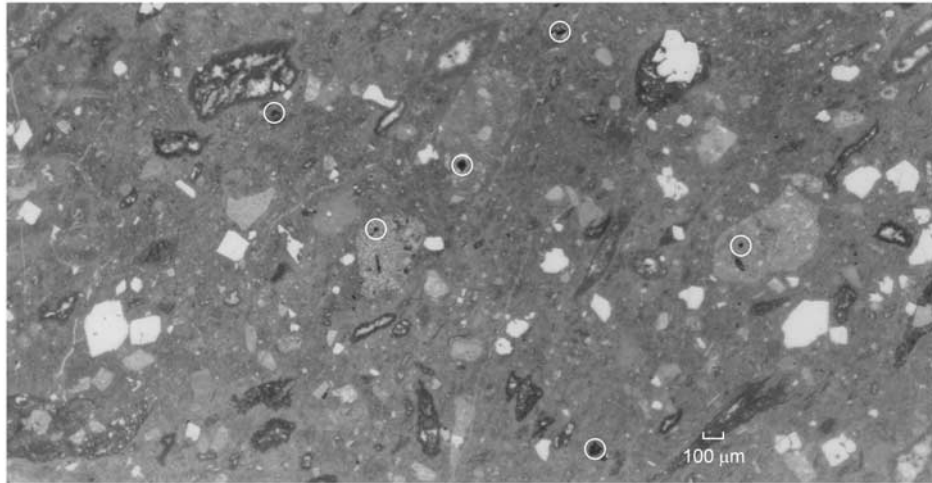
Figure 6. Photomicrograph of NRV02F (Kitchen Creek Rhyolite). Hematite grains present in the volcanic matrix in the size range of 20–60 μm are circled. White circles have diameters equivalent to 100 μm.

The first component (C1) is north with moderate up inclination directions and low to moderate unblocking temperatures and coercivities. A very steep down component with moderate to high unblocking temperatures defines the second component (C2). The third identified component (C3) has high unblocking temperatures and coercivities. This dual-polarity component is directed to the south and down with moderate to fairly steep inclinations. Representative orthogonal plots are shown in Figure 7. Each component is discussed in detail below. All presented paleopoles have been kept in the Australian reference frame.

5.2.1. Viscous Remanent Magnetism (VRM)

[17] Component C1, present in nine sites (33 samples), is directed to the north with a moderate to shallow up direction and is exclusively of normal polarity (Figures 7c–7f, 7h, and 7i). The maximum unblocking temperature/coercivity for this component is 400°C/50 mT; it is generally removed by 250°C, 10 mT, or the LN_2 step. All samples associated with C1 have Koenigsberger ratios of less than 0.1. Although the 95% cone of confidence associated with C1 does not overlap the present field expected at the sample site, it is indistinguishable from the present geocentric axial dipole field and is interpreted to be a viscous remanent magnetization (VRM) acquired during the Brunhes Chron. The mean direction for C1 is Dec = 352°, Inc = −29.4°, k = 38.1, α_{95} = 8.4°. The nine corresponding VGPs yield a mean pole position of 82.1°S, 251.4°E.

5.2.2. Early Permian Primary Remanence and Associated Overprint

[18] A Permian direction, C2, was identified in three paleomagnetic sites from the 293 ± 3Ma Brodies Gap Rhyolite (L. P. Black, as cited by Oversby and Mackenzie [1995]). Orthogonal projection diagrams of demagnetization data for Permian units are defined by a very steep and reversed univectorial decay to the origin with high unblocking temperatures (Figures 7a and 7b). This near-

vertical direction is also present in the bottom-most formation (Bousey Rhyolite) as a presumed remagnetization, with unblocking temperatures ≤500°C. This component is not seen in younger Carboniferous units and the reason for this is unclear, but it may be simply the consequence of thermal instability in this lowest formation for the duration of local volcanism. A statistical comparison of mean directions of the C2 component from the Middle Carboniferous and Permian units indicates that at the 95% confidence interval these two sample sets share a common mean [McElhinny and McFadden, 2000]. Likewise, a comparison of the C2 direction identified in Bousey Rhyolite sites is dissimilar at the 95% confidence interval from the mean C3 component, discussed below. The overall mean direction for C2 is Dec = 207.2°, Inc = 80.3° (k = 60.1, α_{95} = 7.8°, N = 7). The mean paleomagnetic pole calculated from the seven corresponding VGPs lies at 30.9°S, 139.7°E (K = 13.9, A_{95} = 16.8°, angular standard deviation (ASD) = 21.7°) (Figure 8). This paleomagnetic pole is in agreement with previously defined paleogeographic information and paleopoles for Australia in the Early Permian [e.g., Clark and Lackie, 2003].

5.2.3. Middle Carboniferous Primary Remanence

[19] The characteristic remanent magnetization (ChRM) direction, C3, is found in fifteen sites including Carboniferous ignimbrites, a sill associated with early NRV sequences, and as possible remagnetization directions in two sites from the Devonian-Carboniferous Gilberton Formation. As paleomagnetic signatures are temporal, and not necessarily subject to strict geographical boundaries, four of the sixteen original ignimbritic "sample sites" have been grouped for the purposes of VGP calculations (NRVkcr in Table 2). The grouping of NRVkcr was based upon analysis of the paleomagnetic data (tightly clustered, reversed directions) and supported by field evidence that suggests this portion of the field area is dominated by a single ignimbritic cooling sheet and therefore likely to

Table 2. Site-Level Paleomagnetic Results for the Three Components of Magnetization Found in the NRV and Resultant Mean Data[a]

Site	slat (°S)	slong (°E)	n/N	D, deg	I, deg	k	α_{95}, deg	Plat, °S	Plong, °E	Formation
				Component C1						
nrv26	18.5413	143.7486	3/5	1.3	−37.10	45.4	13.0	71.6	276.8	BR
nrv25	18.2810	143.6917	7/11	2.4	−27.65	14.0	16.7	87.3	117.2	RCD/Dike
nrv14	18.3134	143.7717	3/5	6.8	−36.05	27.3	17.3	85.7	356.5	RCD
nrv12	18.3123	143.7815	3/5	352.3	−33.28	75.6	14.3	83.4	69.6	RCD
nrv08	18.3062	143.7472	4/4	342.9	−20.70	20.3	16.7	71.8	256.1	RCD
nrv15	18.3156	143.7623	4/5	346.6	−11.11	22.8	19.7	82.7	233.7	KCR
nrv06	18.2958	143.7312	3/3	356.1	−22.00	17.9	19.5	82.4	293.4	CPr sill
nrv18	17.9715	143.7892	3/5	356.6	−34.00	43.4	12.4	86.8	220	BGR
nrv16	18.3092	143.7497	3/5	324.0	−34.20	19.4	18.7	56.7	227.3	KCR
C1 mean	λ (°S)	φ (°E)	N	R	K	A95°	ASD°		paleolatitude (°S)	
VGP	82.1	251.4	9	8.8	38.1	8.4	13.1		15.7	
				Component C2						
NRV20	17.9806	143.7937	4/4	147.6	73.55	11.9	27.9	42.4	165.4	BGR
NRV19	17.9731	143.7936	4/6	234.6	83.60	13.9	25.5	24.9	132.4	BGR
NRV17	17.9705	143.7892	4/4	223.8	85.59	18.7	21.8	5.2	125.4	BGR
nrv26	18.5413	143.7486	5/5	303.1	78.55	27.0	15.0	24.7	137.1	BR
nrv27	18.5419	143.7505	4/5	216.0	72.78	49.0	10.1	42.9	118.1	BR
nrv28	18.5396	143.7531	3/4	211.0	74.00	233.1	6.5	19.3	163.3	BR
nrv29	18.5393	143.7519	3/3	187.5	73.29	8.6	28.8	49.2	137.9	BR
C2 mean	λ (°S)	φ (°E)	N	R	K	A95°	ASD°		paleolatitude (°S)	
VGP	30.9	139.7	7	6.60	13.9	16.8	21.7		77.0	
				Component C3						
nrv32	18.5422	143.8861	5/5	35.9	−55.9	76.20	8.8	57.7	92.2	DC
nrv30	18.5072	143.7155	5/5	193.4	56.7	422.3	3.7	67.9	114.4	DC
NRV31	18.5447	143.8843	3/3	7.2	−56.7	45.1	12.1	70.2	126.7	BR
NRV29	18.5393	143.7519	3/3	196.9	68.7	37.8	11.7	53.8	126.1	BR
NRV28	18.5396	143.7531	3/4	152.8	65.7	498.0	5.5	53.2	174.5	BR
NRV27	18.5419	143.7505	4/5	211.0	69.9	39.8	19.8	47.4	117	BR
NRV25b	18.2810	143.6917	4/4	348.2	−61.8	134.5	6.0	63.3	163.2	Dike
NRV25a	18.2810	143.6917	5/7	227.8	58.6	41.5	9.8	43.8	91.1	RCD
NRV14	18.3134	143.7717	4/5	205.6	63.9	42.4	14.3	55.4	111.6	RCD
NRV13	18.3134	143.7798	4/5	184.7	55.0	96.0	9.4	72.3	131.1	RCD
NRV12	18.3123	143.7815	5/5	171.8	58.7	157.8	6.2	67.7	160.7	RCD
NRV11	18.3107	143.7822	4/5	165.9	60.9	21.0	20.5	63.5	167.8	RCD
NRV07	18.2972	143.7379	4/5	15.6	−53.4	74.8	8.1	69	105.1	RCD
NRVkcr	18.2900	143.4000	20/20	192.9	59.0	90.9	3.3	65.8	118.6	KCR
NRV10	18.2705	143.8422	5/6	18.6	−58.9	10.8	16.5	68.8	113.2	CPr sill
C3 mean	λ (°S)	φ (°E)	N	R	K	A95°	ASD°		paleolatitude (°S)	
VGP	63.4	125	15	13.6	26.2	7.6	15.8		43	

[a]Paleomagnetic components of the NRV. C1 represents a VRM acquired during the Brunhes Chron. C2 is an assumed Permian paleopole location. C3 is considered to be a primary Middle Carboniferous paleopole. Site, paleomagnetic site mnemonic; slat/slong denote latitude/longitude positions for paleomagnetic sites; n/N represents the number of samples used for analysis and the number of samples collected at individual sites; D, declination; I, inclination; k and α_{95} are calculated Fischer statistics; plat/plong represent the paleopole for each of the site VGPs. Formation identifies from which volcanic unit each site was sampled and are as in Table 1; λ and φ represent the paleopole calculated from site-level VGPs. N and R are the number of VGPs and length of the resultant vector. K, A95, and ASD refer to the precision parameter, half-angle of the 95% confidence cone in degrees; and angular standard deviation in degrees for the associated mean VGP. Paleolatitude is in degrees south as calculated from each mean VGP. Capitalized/lowercased mnemonics in the site column differentiate between assumed primary/secondary magnetizations.

record a single VGP. A combination of field evidence and paleomagnetic results also prompted the splitting of one sample location, NRV25, into two paleomagnetic sites, NRV25a and NRV25b. At this location, a dacitic unit, belonging to the Routh Creek Dacite, was cut by a small basaltic dike and a rhyolitic ring dike. Remanence directions from the dacite (NRV25a) were reversed, while those from the dikes (NRV25b) were of normal polarity.

[20] Normal and reversed polarities, characterized by south and moderate to steep down and north and moderate to steep up inclinations, respectively, are present in C3 (Figures 7c–7i). Of the fifteen paleomagnetic sites used for paleomagnetic analysis, 10 have reversed directions, four record normal directions and one site had mixed polarity. For the mixed polarity site, NRV10, ground cover

obscured the relation between samples and it is recognized that this "mixed polarity" may in fact reflect more than one cooling unit being sampled and/or some degree of overprinting by later flows. As field relations did not allow for the resolution of this problem, the NRV10 direction was calculated using the normal polarity option as the majority of specimens from this site held normal directions. C3 has a mean direction of Dec = 191.4°, Inc = 61.6° (k = 56.48, α_{95} = 5.1°, N = 15). Mean declinations and inclinations are shown in Figure 9. The paleopole calculated from the fifteen corresponding mean VGPs is located at 63.8°S, 124.5°E (K = 26.22, A95 = 7.6°, ASD = 15.8°) (Figure 10). Mean directions and VGPs for C3 are presented in Table 2 (all NRV VGPs are listed as south poles).
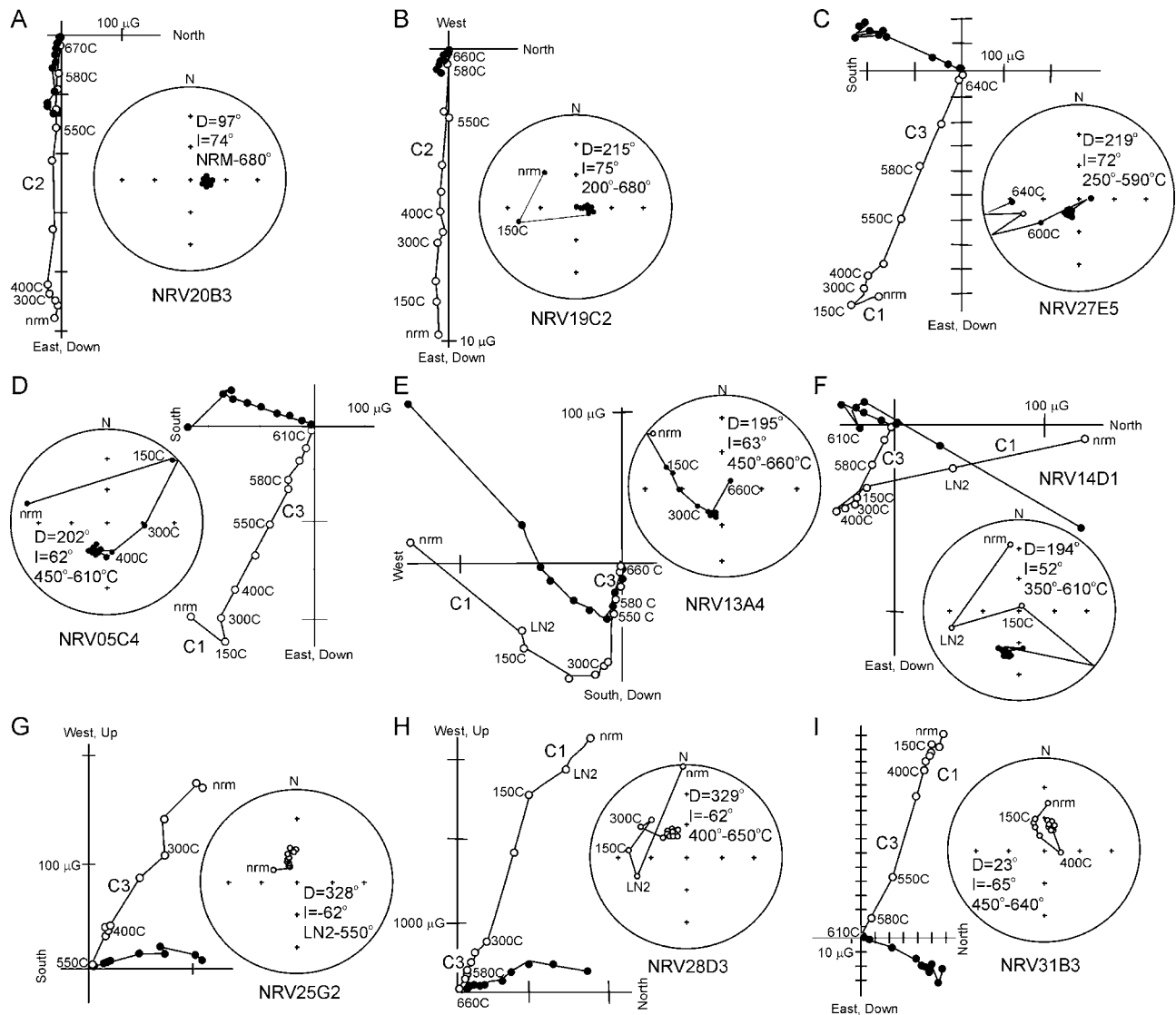
Figure 7. Representative orthogonal plots and corresponding equal-area projection stereonets of thermal demagnetization from nine sites in the NRV. In the orthogonal plots, C1 refers to a viscous remanence, assumed to have been acquired during the Brunhes Chron and is exclusively of normal polarity; C2 is considered to be a primary Permian direction and is characterized by very steep and reversed directions (Figures 7a and 7b, Brodies Gap Rhyolite). C3 is the characteristic remanent magnetization of the NRV and is thought to reflect a primary Middle to earliest Late Carboniferous remanent magnetization. C3 directions are of mixed polarity and steep to moderate inclinations. NRV27E5 (Figure 7c), NRV28D3 (Figure 7h), and NRV31B3 (Figure 7i) are from the Bousey Rhyolite. The Kitchen Creek Rhyolite is represented by NRV05C4 (Figure 7d). Figures 7e and 7f are results from the Routh Creek Dacite. Results from a ring dike associated with the Routh Creek Dacite are shown in Figure 7g. Although pictured in the volcanostratigraphic column (Figure 2) samples from the Corkscrew Rhyolite did not yield consistent paleomagnetic results and were not included in analysis. C2 or C3 declination and inclination directions are cited for each stereographic projection, with the relevant temperature range.
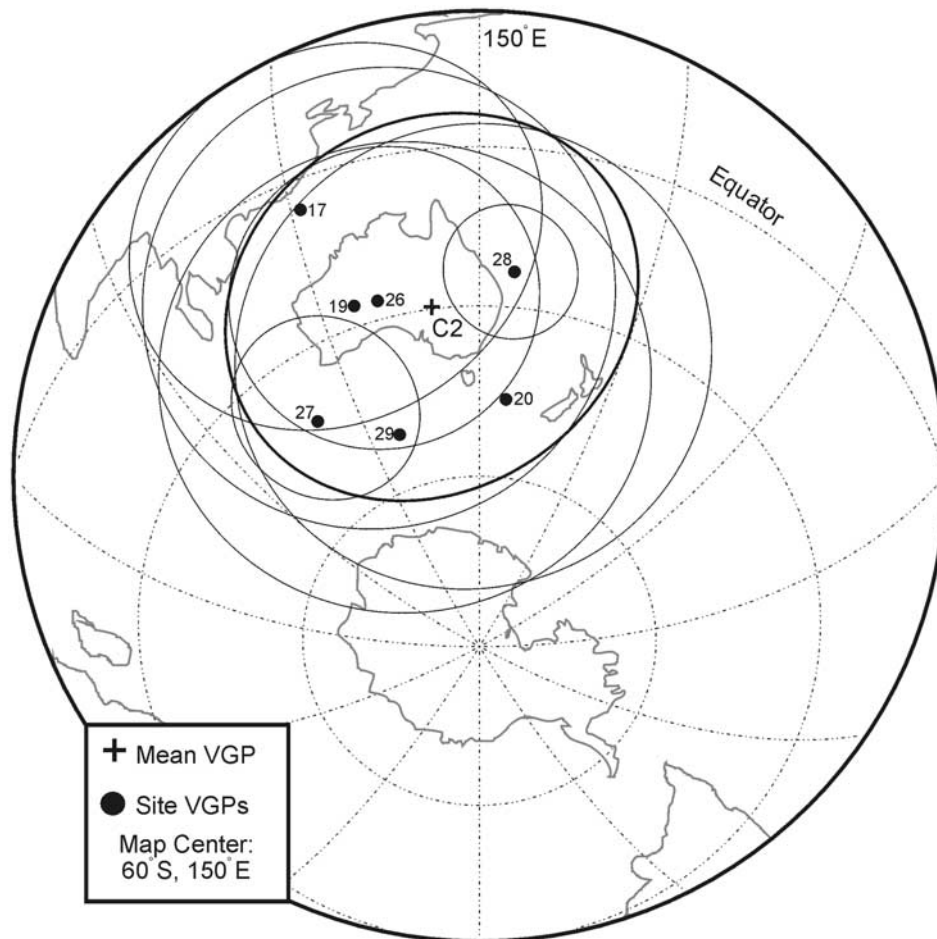
Figure 8. VGPs of the C2, Permian, component. The cross just off 30°S, in southern Australia, represents the mean direction of C2 VGPs. C2 has a mean direction of Dec = 207.2°, Inc = 80.3° (k = 60.1, α_{95} = 7.8). The corresponding mean VGP, calculated from the seven associated VGPs lies at 30.9°S, 139.7°E (K = 13.9, A_{95} = 16.8°). Solid circles and corresponding numbers relate to site-level VGP directions, and dm/dp ovals of confidence are also shown for each VGP. The thicker dm/dp oval corresponds to the mean C2 result. Data for C2 are listed in Table 2. Plot is an equal-area projection with map center located at 60°S, 150°E, modified from GMAP-32 [*Torsvik and Smethurst*, 1989–1997].

[21] Polarity horizons for the three volcanic formations investigated provide a good age constraint for the onset of the PCRS. The 323 ± 3 Ma Bousey Rhyolite has only normal polarities while the Routh Creek Dacite, 322 ± 6.6 Ma, displays both normal and reversed directions. The youngest of the three formations, the 317 ± 6.3 Ma Kitchen Creek Rhyolite, is of exclusive reverse polarity. This is consistent with recent reassessments of the onset of the PCRS dating possibly to the Bashkirian (~314 Ma) or older [*Derder et al.*, 2001; *Opdyke et al.*, 2000]. Field tests were not possible as a part of this investigation, but the C3 component does pass a reversal test of the two polarity means. A relatively small sample size ($N_{reversed}$ = 10, N_{normal} = 5) coupled with two sample sets that do not share a common precision, prompted the use of a bootstrap reversal test [*McElhinny and McFadden*, 2000; *Tauxe*, 1998] to compare the reversed and normal mean directions associated with C3. When the normal data are inverted to their reversed antipode, the sample sets are shown to be indistinguishable at the 95% confidence interval, indicating that the normal and reversed poles are likely to be from the same population.

6. Discussion

[22] The C3 component is defined by extremely stable thermal and AF demagnetization curves. Rock magnetic experiments attest to the NRV remanence carrier being an excellent paleomagnetic recorder. Koenigsberger ratios $Q \geq 3$ for those samples that did not contain secondary magnetizations indicate that remanent magnetization is dominant in these volcanics and suggests that the remanence carriers are predominantly in the PSD size range and should, therefore, be capable of retaining magnetizations that are stable over geological timescales. The C3 component of the NRV passes the bootstrap reversal test at the 95% confidence interval and polarities are formation specific. Analysis of this ChRM indicates that it is dissimilar at
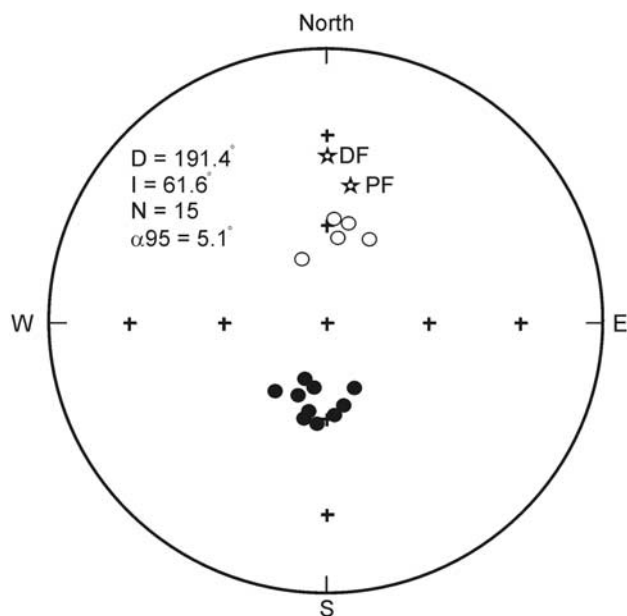
Figure 9. Equal-area projection of site-level declinations and inclinations for C3 components. Stars represent locations of the best fit dipole field (DF) and the present geomagnetic field (PF). Filled and open circles correspond to reversed and normal polarities, respectively. The mean direction of C3 is Dec = 191.4°, Inc = 61.6° (k = 56.48, α_{95} = 5.1°). When normal directions are inverted to the reversed antipode, the sample sets are indistinguishable at the 95% confidence interval.

the 95% confidence interval from the present-day axial dipole field and the present geomagnetic field expected at the sample site. An ASD of 15.8° is consistent with the 0–5 Ma window estimates of ASD based on modern secular variation [*Butler*, 1992; *Merrill and McElhinny*, 1983], suggesting secular variation for the NRV ignimbrites has been sufficiently averaged. Dual polarity of the ignimbritic sequences and an eruption life of roughly 8 m.y. for sampled portions of this caldera system also impart support for secular variation having been sufficiently averaged for the NRV.

[23] A revised Carboniferous APWP for Australia is shown in Figure 11. Corresponding paleopoles are listed in Table 3. The Middle to Late Carboniferous segment of this pole path differs from previously published paths [e.g., *Chen et al.*, 1993; *Li and Powell*, 2001; *Schmidt and Clark*, 2000] in that it plots significantly south (present-day Australian coordinates) of the syndeformational Mount Eclipse Sandstone poles, mes1 and mes2 [*Chen et al.*, 1994; *Li et al.*, 1989], which are associated with the Middle Carboniferous Alice Springs Orogeny in central Australia. The discrepancy between the NRV pole and the syndeformational mes1 and mes2 poles may arise from poorly constrained paleohorizonatal or diachronous folding for the Mount Eclipse Sandstone and a possibly overly steep bias to the pole path introduced by NRV.

[24] An examination of Figure 11 and Table 3 also raises questions as to the differences between the well-defined BAT paleopole and that of NRV. If median magnetization ages for these two poles, ~325Ma and ~321Ma, respectively, are used in analysis of the presented APWP, the suggested drift of nearly 50° could not be substantiated. However, a slightly more liberal interpretation, incorporating the Bathurst Batholith (BAT), Connors Volcanics (COV), NRV, and Mount Leyshon Igneous Complex/Tuckers Range Volcanics (MTL) poles over a period of some 40 m.y., documents Australia's migration from a subequatorial position to latitudes in excess of 60°S. This associated 60°+ of polar wander, equivalent to about 15–20 cm yr^{-1}, is consistent with Gondwana's rapid clockwise rotation during the Carboniferous as Western Gondwana moved from high to low latitudes with Eastern Gondwana moving in the opposite sense [e.g., *Aïfa et al.*, 1990; *Chen et al.*, 1994; *Derder et al.*, 1994].

[25] A comparison of available high quality Carboniferous Western Gondwanan paleopoles and the revised Australian APWP highlights the agreement between the presented pole path and data from the far side of Gondwana (see Figure 11). Western Gondwanan poles have been rotated into Australian coordinates using the reconstruction parameters of *Powell and Li* [1994] and are presented in Table 4. The similarity between the NRV pole and those from Western Gondwana lends credence to the claim of the primary remanence for the ~320 Ma NRV paleopole. In light of the consistency between the NRV and Western Gondwanan data, in conjunction with the evidence presented above, it seems most likely that the lack of agreement between the APWP presented herein and earlier investigations may simply be the result of the scarcity of similarly aged paleopoles from Australia that have escaped remagnetization. Interestingly, however, the presented APWP does accommodate results from the recently revisited Tamworth Belt of eastern Australia's New England orogen [*Opdyke et al.*, 2000] (RCW pole in Figure 11 and Table 3). The position of the 318–306 Ma RCW pole with respect to the 325–317 Ma NRV and 280–292 Ma MTL paleopoles in Figure 11 may support *Opdyke et al.*'s [2000] account of this region having largely escaped regional Early Permian remagnetization documented by *Lackie and Schmidt* [1993].

7. Conclusions

[26] As APWPs reflect a continent's position through time, the one proposed in Figure 11 documents Eastern Gondwana's clockwise rotation and migration to high latitudes during the Late Paleozoic. The Middle to Late Carboniferous was a time of global plate reorganization, dominated by the collision of two supercontinents, Gondwana and Laurasia, and the formation of Pangea. This collision is reflected in the presented APWP wherein Eastern Gondwana is drifting southward during the Early to Middle Carboniferous undergoes fairly rapid clockwise rotation in the Late Carboniferous and then continues high latitude drift into the Early Permian. Locally, the distinct tectonic elements of the Kennedy Volcanic Province, e.g., the dominance of highly silicic ignimbrites, attributed to Carboniferous mantle upwelling, followed by Permian
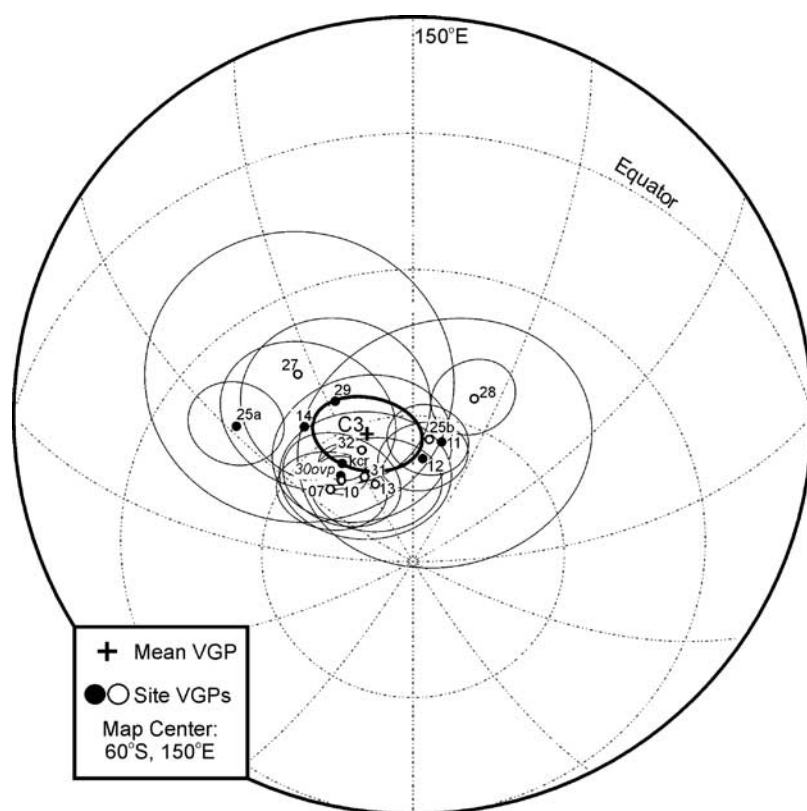
Figure 10. Mean C3 direction and corresponding VGPs. Cross near C3 marks location of mean paleopole for the NRV at 63.8°S, 124.5°E (K = 26.22, A_{95} = 7.6°, ASD = 15.8°), related confidence oval is marked by a slightly thicker line than for individual VGPs. Solid and open circles with associated numbers refer to reversed and inverted normal VGPS, respectively, for sites listed in Table 2, defining the C3 direction. Plot is an equal-area projection with map center located at 60°S, 150°E. Modified from GMAP-32 [*Torsvik and Smethurst*, 1989–1997].

extension, may reflect far-field effects of this collision and a shift in the paleogeodynamics regime on the Eastern Gondwanan margin.

[27] Recent analysis of Late Carboniferous-Early Triassic (300–140 Ma) paleomagnetic data from North America and Europe [*Van der Voo and Torsvik*, 2001] highlight the growing concern over the biasing of paleomagnetic data by significant (and generally unrecognized) contributions from nondipole components of the Earth's paleofield. Although the work presented by *Van der Voo and Torsvik* [2001] is not temporally relevant to the data presented herein, it is recognized that the deviation from previous pole paths presented by this study could be an artifact of the NRV having formed at midpaleolatitudes and, therefore, highly susceptible to biasing by octupolar fields. If the NRV paleomagnetic pole was biased by some 10°–15°, then the more conventional Australian APWP could be still viable and Australia would have occupied subpolar latitudes by the Early Carboniferous. However, the general agreement between the NRV pole and similarly aged poles from Western Gondwana may suggest minimal contribution from octupolar fields during this time as one would not necessarily expect such conformity between equatorial data (coming from northern Africa), polar data (southern Chile) and

that obtained from midpaleolatitudes (Argentina, Brazil and Australia).

[28] The high-quality paleomagnetic data obtained from the NRV and detailed rock magnetic tests testify to the NRV being an excellent paleomagnetic recorder that is stable over geologic time. Dual polarity magnetizations spanning some 8m.y. also support the integrity with which these volcanics record ancient fields and the exclusive reversed polarity of the 316.9 ± 6.3 Ma Kitchen Creek Rhyolite, and younger sampled units, is consistent with the recent refinements offered by *Opdyke et al.* [2000] with respect to the base of the PCRS in Australia. However, while the NRV pole is well defined and agrees well with tightly grouped Middle to Late Carboniferous paleopoles from Western Gondwana, it is acknowledged that this pole may introduce an overly steep bias to the Australian APWP during this period.

[29] *Chen et al.* [1994] recognized the necessity for more high quality paleomagnetic poles from the Middle Carboniferous to resolve timings associated with the closure of the ocean basin separating Gondwana and Laurasia and the formation of Pangea. The ∼320 Ma NRV pole presented here represents one step in this process. This pole is temporally well constrained, statistically well defined and it is consistent with paleopoles from Western
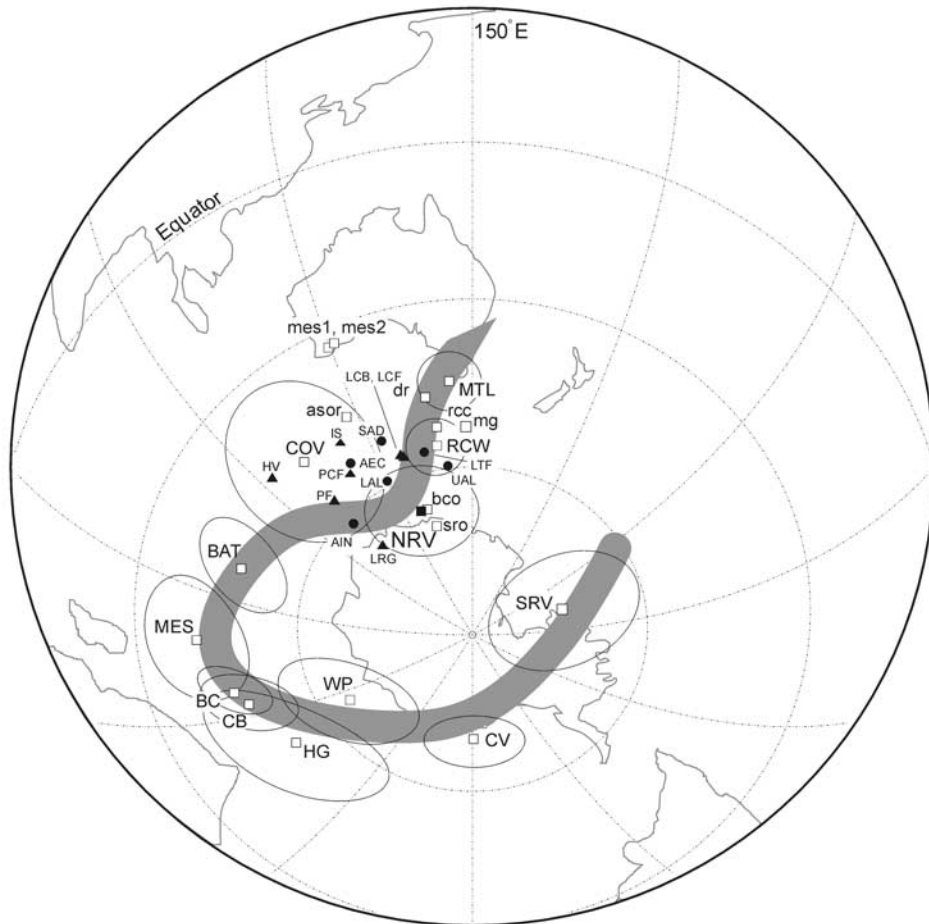
Figure 11. Revised Carboniferous APWP for Australia from the Early Devonian through the Early Permian. Australian paleopoles are marked by open squares. The mean NRV C3 paleopole is a filled square. Lowercase mnemonics refer to paleopoles that are thought to be magnetically overprinted. These paleopoles are included only as a means of showing their relation to the presented APWP and were not used in the construction of this polepath. Paleopoles from Western Gondwana are included for comparison. Solid triangles/circles correspond to paleomagnetic data from South America/Africa, respectively. The Middle to earliest Late Carboniferous portion of this APWP differs from previously published APWPs for Australia in that it incorporates a marked southerly swing between the BAT and MTL paleopoles, implying that Eastern Gondwana remained at midlatitudes into the earliest Late Carboniferous, not crossing into subpolar latitudes until about 310 Ma, signified by the RCW paleopole. Table 4 lists all paleopole information used for the compilation of this APWP. Plot is an equal-area projection with map center located at 60°S, 150°E. Modified from GMAP-32 [*Torsvik and Smethurst*, 1989–1997].

Table 3. Paleomagnetic Poles Used in the Construction of the APWP Presented in Figure 11[a]

Formation	Mnemonic	Slat, °N	Slong, °E	Rplat, °S	Rplong, °E	k	α_{95} deg	Dp, deg	Dm, deg	Age of Magnetization	Q Value	GPMDB Ref or. Reference
Mount Leyshon Intrusive Complex	MTL	−20.3	146.3	43	137	53.5	3	6	6	280–292	6	*Clark and Lackie* [2003]
Serie d'Abadla, Upper Unit	SAD	31.0	357.3	52.0	124.7	59	6	5	5	256–290	5	1459
La Colina Basalt	LCB	−30.1	292.6	54.6	127.3	NG[b]	5	6.9	6.9	295–305	3	178
Lago Ranco Granites	LRG	−40.2	287.7	66.9	102.0	25.2	12.3	18.8	18.8	295–310	5	2285
Lower Tiguentourine Formation	LTF	27.7	9.0	53.7	132.4	170	4	5	5	280–300	5	2728
Upper El Adeb Larache Formation	UAL	27.5	8.9	58.6	138.2	837	2	2	2	270–303	5	2540
Rocky Creek Conglomerate	rcc[c]	−30.0	150.3	51	138	79	7	17	17	290–323	-	304
Main Glacial Stage	mg[c]	−32.6	151.7	53	149	33	6	11	11	290–323	-	304
Dotswood Redbeds	dr[c]	−19.8	146.4	46.1	135.6	17.4	8.2	13.7	15	C/P?	-	406
Pular and Cas Formations	PCF	−24.0	291.5	52.6	112.4	NG[b]	9	9	13	290–323	6	1420
Itarare Subgroup, Tubarao Group	IS	−21.0	312.8	48.9	114	NG[b]	11	15	15	290–323	3	798
Snowy River Volcanics	sro[c]	−37.5	148.2	68	132	26.5	3	5	5	290–323	-	1365
Buchan Caves Limestone	bco[c]	−37.4	148.3	64	127	719	2	4	4	290–323	-	1365
Lower El Adeb Larache Formation	LAL	27.4	8.9	54.7	120.1	161	3	2	2	303–311	5	2540
Ain Ech Chebbi, Hassi Bachir Formations	AEC	26.6	1.0	53.3	114.3	127.8	4	3	3	307–325	4	1629
Mt Eclipse Sandstone, syndeformational	mes1[c]	−22.6	132.0	32	119	68.9	6	11	11	300–340	-	2866
Mt Eclipse Sandstone, syndeformational	mes2[c]	−22.3	131.3	33	121	14	10	19	19	300–340	-	2185
Alice Springs Orogeny	asor[c]	−23.6	134.5	45.8	118.1	14	2.9	5	5.4	305–315	-	1769
La Colina Formation	LCF	−30.0	293.0	54.4	127.3	NG[b]	0	5	5	290–323	6	1144
Piaui Formation	PF	−5.0	317.0	54.1	99.5	NG[b]	16	18	24	300–323	3	613
Rocky Creek and Werrie Synclines	RCW	−31.0	150.5	51.9	141.2	8	5.7	NG[b]	NG[b]	306–319	7	*Opdyke et al.* [2000]
Hoyada Verde Formation	HV	−31.7	290.5	43	94.0	38	5	6	8	290–323	5	2648
Connors Volcanics	COV	−22.5	149.3	46	100	17.9	10	13	16	310–330	5	3265
Newcastle Range Volcanics	NRV	−18.3	143.7	63.8	124.5	56.48	5.1	6.1	7.9	317–325	6	*this study*
Ain Ech Chebbi, Middle Carboniferous	AIN	26.5	0.5	60.6	105.2	383	4.7	NG[b]	NG[b]	L.Serpukhovian	7	*Derder et al.* [2001]
Bathurst Batholith	BAT	−33.5	150.0	45	71	NG[b]	7	6	10	319–332	7	3264
Mount Eclipse Sandstone	MES	−22.6	132.0	37	52	68.9	8	8	8	339–350	7	2866
Brewer Conglomerate	BC	−23.9	133.7	47	41	86.7	6	6	6	363–367	7	2726
Hervey Group	HG	−33.2	148.5	54	24	13.8	15	8	16	363–367	5	1579
Reef Complex, Canning Basin	CB	−18.3	125.6	49.1	38	61.6	7.8	4.7	8.3	363–377	6	1345
Worange Point Formation	WP	−36.9	149.9	67	28	15.9	10	10	10	363–367	5	2191
Comerong Volcanics	CV	−35.5	150.0	76	330	38.8	7	7	7	370–379	6	1565
Snowy River Volcanics	SRV	−37.5	148.2	74	222	25.6	9	10	14	391–417	7	1365

[a]Mnemonic refers to the paleopole designators in Figure 11. Slat/Slong are site latitude/longitude; Rplat/Rplong are paleopoles locations, rotated into the Australian reference frame, if necessary; k is the precision parameter given in each study; α_{95} is the half-angle of the 95% circle of confidence associated with each paleomagnetic pole, Dm/Dp correspond to the semiaxes of uncertainty associated with each calculated paleopole at the 95% confidence interval, Dp is related to uncertainty in the colatitude; Dm is orthogonal to Dp; age of magnetization refers to the presumed age of remanence; Q value describes quality criteria of *Van der Voo* [1990], paleopoles with Q ≥ 3 were considered for analysis; and GPMDB Ref. No. or Reference correspond to the reference number given in the Global Paleomagnetic Database (http://www.ngu.no/dragon/Palmag/paleomag.htm) or the journal reference of data not yet assigned a reference number in the database. All paleomagnetic poles have been rotated into the Australian reference frame. Rotation parameters are modified from those given by *Powell and Li* [1994] and are provided in Table 4.

[b]NG indicates that these values were not given in the original study.

[c]Lowercased mnemonics represent data that are thought to be paleomagnetically overprinted; Q values were not assigned to these data, nor were they used in the generation of the APWP presented in Figure 11.

Gondwana and Late Paleozoic glacial centers [*Caputo and Crowell*, 1985]. Up until the NRV paleopole, the Visean Mount Eclipse Sandstone (MES) pole represented the youngest extant paleopole from Paleozoic cratonic Australia (discounting those with paleomagnetic histories irreversibly obscured by remagnetization events). Widespread glaciation in the Late Carboniferous is thought to have removed much of the older sedimentary rock record and the nearly ubiquitous Permian remagnetizations have eliminated much of the paleomagnetic record in units associated with the New England Fold Belt in southeastern Australia [*Lackie and Schmidt*, 1993]. Paleomagnetic results from the Middle to earliest Late Carboniferous Newcastle Range Volcanics suggest that the Kennedy Volcanic Province, of which the NRV is a remnant, may

be well suited to more detailed investigation as it represents an igneous overprinting of cratonic Australia during this time, was free from glaciation, and may have escaped the pervasive Permian remagnetizations.

Table 4. Euler Data Used to Rotate Western Gondwanan Paleopoles Into the Australian Reference Frame[a]

Rotation Pir	Latitude, °N	Longitude, °E	Angle, deg
Africa to Australia	29.94	119.84	52.81
South America to Australia	51.01	46.45	69.5

[a]Poles used for paleomagnetic pole rotations of African and South American data into the Australian reference frame. Modified from Table 1 of *Powell and Li* [1994].

References

Aïfa, T., H. Feinberg, and J.-P. Pozzi, Devonian-Carboniferous paleopoles for Africa; consequences for Hercynian geodynamics, *Tectonophysics*, *179*, 287–300, 1990.

Belousova, E. A., W. L. Griffin, S. R. Shee, S. E. Jackson, and S. Y. O'Reilly, Two age populations of zircons from the Timber Creek kimberlites, Northern Territories, Australia, as determined by laser-ablation ICPMS analysis, *Aust. J. Earth Sci.*, *48*, 603–619, 2001.

Butler, R. F., *Paleomagnetism: Magnetic Domains to Geologic Terranes*, 319 pp., Blackwell, Malden, Mass., 1992.

Caputo, M. V., and J. C. Crowell, Migration of glacial centers across Gondwana during the Paleozoic, *Geol. Soc. Am. Bull.*, *96*, 1020–1036, 1985.

Chen, Z., Z. X. Li, C. M. Powell, and B. E. Balme, Palaeomagnetism of the Brewer Conglomerate in central Australia, and fast movement of Gondwanaland during the Late Devonian, *Geophys. J. Int.*, *115*, 564–574, 1993.

Chen, Z., Z. X. Li, C. McA. Powell, and B. E. Balme, An Early Carboniferous paleomagnetic pole for Gondwanaland: New results from the Mount Eclipse Sandstone in the Ngalia Basin, central Australia, *J. Geophys. Res.*, *99*, 2909–2924, 1994.

Clark, D. A., Magnetic petrophysics and magnetic petrology: Aids to geological interpretation of magnetic surveys, *J. Aust. Geol. Geophys.*, *17*, 83–103, 1997.

Clark, D. A., and M. A. Lackie, Palaeomagnetism of the Early Permian Mount Leyshon Intrusive Complex and Tuckers Igneous Complex, North Queensland, Australia, *Geophys. J. Int.*, in press, 2003.

Constable, C., and L. Tauxe, The bootstrap for magnetic susceptibility tensors, *J. Geophys. Res.*, *95*, 8383–8395, 1990.

Derder, M. E., B. Henry, N. Maeabet, and L. Daly, Palaeomagnetism of the Stephano-Autunian Lower Tiguentourine formations from stable Saharan craton (Algeria), *Geophys. J. Int.*, *116*, 12–22, 1994.

Derder, M. E. M., B. Smith, B. Henry, A. K. Yelles, B. Bayou, H. Djellit, R. Aitouali, and H. Gandriche, Juxtaposed and superimposed paleomagnetic primary and secondary components from the folded middle Carboniferous sediments in the Reggane Basin (Saharan craton, Algeria), *Tectonophysics*, *332*, 403–421, 2001.

Dunlop, D. J., and Ö. Özdemir, *Rock Magnetism: Fundamentals and Frontiers*, 573 pp., Cambridge Univ. Press, New York, 1997.

Fisher, R. A., Dispersion on a sphere, *Proc. R. Soc. London, Ser. A*, *217*, 295–305, 1953.

Kirschvink, J. L., The least-squares line and plane and the analysis of palaeomagnetic data, *Geophys. J. R. Astron. Soc.*, *62*, 699–718, 1980.

Kletetschka, G., P. J. Wasilewski, and P. T. Taylor, Unique thermoremanent magnetization of multidomain size hematite: Implications for magnetic anomalies, *Earth Planet. Sci. Lett.*, *176*, 469–479, 2000.

Lackie, M. A., and P. W. Schmidt, Remagnetisation of strata during the Hunter-Bowen Orogeny, *Explor. Geophys.*, *24*, 269–274, 1993.

Li, Z. X., and C. M. Powell, An outline of the palaeogeographic evolution of the Australasian region since the beginning of the Neoproterozoic, *Earth Sci. Rev.*, *53*, 237–277, 2001.

Li, Z. X., C. M. Powell, and P. W. Schmidt, Syn-deformational remanent magnetization of the Mount Eclipse Sandstone, central Australia, *Geophys. J. Int.*, *99*, 205–222, 1989.

Li, Z. X., C. M. Powell, and D. G. Morris, Syn-deformational and drilling-induced remanent magnetizations from diamond drill cores of the Mt Eclipse Sandstone, central Australia, *Aust. J. Earth Sci.*, *38*, 473–484, 1991.

Lowrie, W., Identification of ferromagnetic minerals in a rock by coercivity and unblocking temperature properties, *Geophys. Res. Lett.*, *17*, 159–162, 1990.

McElhinny, M. W., and P. L. McFadden, *Paleomagnetism: Continents and Oceans*, 387 pp., Academic, San Diego, Calif., 2000.

Merrill, R. T., and M. W. McElhinny, *The Earth's Magnetic Field: Its History, Origin and Planetary Perspective*, 401 pp., Academic, San Diego, Calif., 1983.

Opdyke, N. D., J. Roberts, J. Claoué-Long, E. Irving, and P. J. Jones, Base of the Kiaman: Its definition and global stratigraphic significance, *Geol. Soc. Am. Bull.*, *112*, 1315–1341, 2000.

Oversby, B., and D. Mackenzie, Geology of the Late Palaeozoic ignimbrites and associated rocks in the Georgetown Region, northeastern Queensland, *AGSO Rec. 1994/20*, 1–78, 1995.

Powell, C. M., and Z. X. Li, Reconstruction of the Panthalassan margin of Gondwanaland, in *Permian-Triassic Pangean Basins and Foldbelts Along the Panthalassan Margin of Gondwanaland*, edited by J. J. Veevers and C. M. Powell, *Mem. Geol. Soc. Am.*, *184*, 5–9, 1994.

Schmidt, P. W., Palaeomagnetic cleaning strategies, *Phys. Earth Planet. Inter.*, *76*, 169–178, 1993.

Schmidt, P. W., and D. A. Clark, Paleomagnetism, apparent polar-wander path & paleolatitude, in *Billion-Year Earth History of Australia and Neighbors in Gondwanaland*, edited by J. J. Veevers, pp. 12–17, GEMOC Press, Sydney, 2000.

Schmidt, P. W., B. J. J. Embleton, and H. C. Palmer, Pre and post folding magnetization from the Devonian Snowy River Volcanics and Buchan Caves Limestone, Victoria, *Geophys. J. R. Astron.*, *91*, 155–170, 1987.

Tauxe, L., *Paleomagnetic Principles and Practice*, 299 pp., Kluwer Acad., Norwell, Mass., 1998.

Torsvik, T., and M. Smethurst, GMAP-32, Geographic mapping and meconstruction system, Geol. Surv. of Norway, Oslo, 1989–1997.

Van der Voo, R., The reliability of palaeomagnetic poles, *Tectonophysics*, *184*, 1–9, 1990.

Van der Voo, R., *Paleomagnetism of the Atlantic, Tethys, and Iapetus Oceans*, 411 pp., Cambridge Univ. Press, New York, 1993.

Van der Voo, R., and T. Torsvik, Evidence for Permian and Mesozoic non-dipole field provides an explanation for the Pangea reconstruction problems, *Earth Planet. Sci. Lett.*, *187*, 71–81, 2001.

Zijderveld, J. D. A., A. C. demagnetization of rocks: Analysis of results, in *Methods in Palaeomagnetism*, edited by D. W. Collinson, K. M. Creer, and S. K. Runcorn, pp. 254–286, Elsevier Sci., New York, 1967.

—————————————

K. L. Anderson, Department of Earth and Environmental Sciences, Geophysics Section, Ludwig-Maximilians-Universität; Theresienstrasse 41, D-80333 Munich, Germany. (kari@geophysik.uni-muenchen.de)

D. A. Clark and P. W. Schmidt, CSIRO Division of Exploration and Mining, North Ryde, New South Wales 2113, Australia. (David.Clark@csiro.au; Phil.Schmidt@csiro.au)

M. A. Lackie, Department of Earth and Planetary Sciences, Macquarie University, Sydney, New South Wales 2109, Australia. (mlackie@laurel.ocs.mq.edu.au)